

# Tunable Low-Relative Humidity and High-Capacity Water Adsorption in a Bibenzotriazole Metal-Organic Framework

Dalal Alezi,<sup>||</sup> Julius J. Oppenheim,<sup>||</sup> Patrick J. Sarver,<sup>||</sup> Andrei Iliescu, Bhavish Dinakar, and Mircea Dincă\*



Cite This: *J. Am. Chem. Soc.* 2023, 145, 25233–25241



Read Online

ACCESS |



Metrics & More

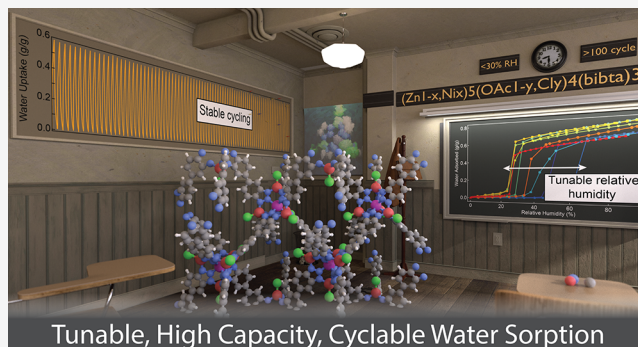


Article Recommendations



Supporting Information

**ABSTRACT:** Materials capable of selectively adsorbing or releasing water can enable valuable applications ranging from efficient humidity and temperature control to the direct atmospheric capture of potable water. Despite recent progress in employing metal-organic frameworks (MOFs) as privileged water sorbents, developing a readily accessible, water-stable MOF platform that can be systematically modified for high water uptake at low relative humidity remains a significant challenge. We herein report the development of a tunable MOF that efficiently captures atmospheric water (up to 0.78 g water/g MOF) across a range of uptake humidity (27–45%) employing a readily accessible Zn bibenzotriazolate MOF, CFA-1 ( $[\text{Zn}_5(\text{OAc})_4(\text{bibta})_3]$ ,  $\text{H}_2\text{bibta} = 1H,1H'-5,5'$ -bibenzo[d][1,2,3]triazole), as a base for subsequent diversification. Controlling the metal identity (zinc, nickel) and coordinating nonstructural anion (acetate, chloride) via postsynthetic exchange modulates the relative humidity of uptake, facilitating the use of a single MOF scaffold for a diverse range of potential water sorption applications. We further present a fundamental theory dictating how continuous variation of the pore environment affects the relative humidity of uptake. Exchange of substituents preserves capacity for water sorption, increases hydrolytic stability (with 5.7% loss in working capacity over 450 water adsorption-desorption cycles for the nickel-chloride-rich framework), and enables continuous modulation for the relative humidity of pore condensation. This combination of stability and tunability within a synthetically accessible framework renders Ni-incorporated  $\text{M}_3\text{X}_4\text{bibta}_3$  promising materials for practical water sorption applications.



Tunable, High Capacity, Cyclable Water Sorption

## INTRODUCTION

The use of reticular chemical principles within metal-organic framework (MOF) syntheses has enabled the creation of tailored materials with enhanced properties and performance, expanding the range of applications of MOFs. An increasing number of studies have broadly investigated the use of MOFs for water adsorption, leveraging their tunable microporosity, steep water uptake due to uniform pore size, and the presence of potential binding groups, to facilitate atmospheric water harvesting, desiccation, moisture control, and refrigeration.<sup>1–4</sup> As a result, MOFs have emerged as promising candidates for addressing challenges related to water management and environmental sustainability.

Designing ideal water sorbent materials for a given application necessitates optimization of several key parameters, including stability over cycling, relative humidity of pore condensation, working capacity, kinetics of cycling, environmental impact of the material and its synthesis, and costs associated with MOF synthesis and use. Considering these requirements in mind, advancements in reticular chemical methods have led to the development of stable and porous frameworks with high water uptake. Furthermore, several research studies have demonstrated the importance of altering

the hydrophilicity of the pore interior to effectively modulate the specific relative humidity (RH) at which pore condensation occurs (the relative humidity at half-capacity is denoted as  $\alpha$ ). This hydrophilicity can be modified through various approaches, including ligand functionalization,<sup>5</sup> cation/anion exchange,<sup>2,6</sup> and, more recently, by varying the incorporation of organic linkers in multivariate MOFs.<sup>7,8</sup> These variations have enabled shifts in the relative humidity for pore condensation up to 30% relative humidity. We envisioned that systematically modifying a single, synthetically accessible MOF scaffold derived from inexpensive feedstocks could provide an ideal approach to practically valuable MOF water sorption, enabling large-scale deployment of materials tailored to specific applications. The key to addressing this challenge has been identifying a MOF that could be synthesized from

Received: August 2, 2023  
Revised: October 13, 2023  
Accepted: October 25, 2023  
Published: November 13, 2023



inexpensive precursors and capable of undergoing efficient modification to afford a range of diverse derivatives.

The Zn bibenzotriazolate MOF CFA-1 ( $[\text{Zn}_5(\text{OAc})_4(\text{bibta})_3]$ ,  $\text{H}_2\text{bibta} = 1\text{H},1\text{H}'\text{-}5,5'\text{-bibenzo[d]-[1,2,3]triazole}$ )—a material known to undergo efficient metal and anion exchange to provide access to a range of pore environments<sup>9</sup>—appears perfectly suited to serve as a convenient platform for the synthesis of a range of materials with tunable water sorption properties. Further, the  $\text{H}_2\text{bibta}$  linker is derived from an industrially produced monomer already generated on multiton scale annually, ensuring that any developed materials could be efficiently and economically scaled up (Figure 1d).<sup>10</sup> Additionally, given that  $\text{H}_2\text{bibta}$  is a

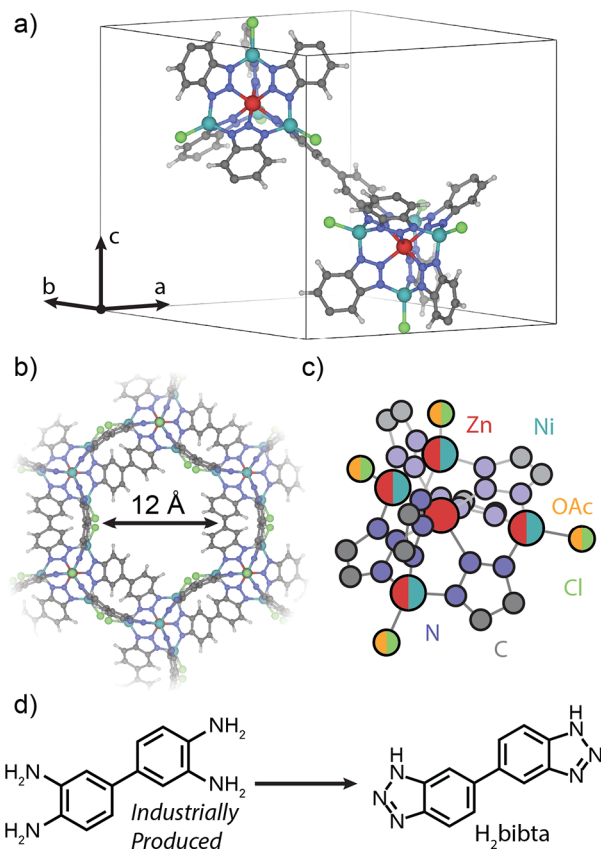


**Figure 1.** (a) Model of unit cell for  $\text{M}'\text{M}_4\text{X}_4(\text{bibta})_3$ ; (b) view of  $\text{M}'\text{M}_4\text{X}_4(\text{bibta})_3$  down the  $c$ -axis; (c) Kuratowski-cluster SBU and summary of synthetic modifications explored in this study; (d) structure and synthetic schematic of organic linker.

triazolate-based linker, it should form robust chemical bonds with late transition metals, giving rise to hydrolytically stable MOFs, which is an essential parameter for practical water adsorption applications. Here, we report methods of accessing highly porous, hydrolytically stable, and scalable  $\text{M}'\text{M}_4\text{X}_4\text{bibta}_3$  ( $\text{M}' = \text{Zn}$ ;  $\text{M} = \text{Zn}, \text{Ni}$ ;  $\text{X} = \text{Cl}, \text{OAc}$ ) frameworks (Figure 1a–c) and demonstrate that these materials capture water vapor at a broad range of uptake humidities (27–64% RH) with high water uptake capacities (up to  $0.78 \text{ g}_{\text{H}_2\text{O}}/\text{g}_{\text{MOF}}$ ). Exchanging the majority of accessible zinc atoms provides efficient access to  $[\text{Ni}(74\%), \text{Cl}(92\%)]$ , a particularly valuable sorbent with a capacity of  $0.78 \text{ g/g}$ , uptake humidity of 27%, and hydrolytic stability over 450 water adsorption–desorption cycles.

## RESULTS AND DISCUSSION

### Synthesis and Post-Synthetic Exchange.

$\text{Zn}_5(\text{OAc})_4(\text{bibta})_3$  (CFA-1;  $\text{bibta}^{2-} = 5,5'$ -bibenzotriazolate,

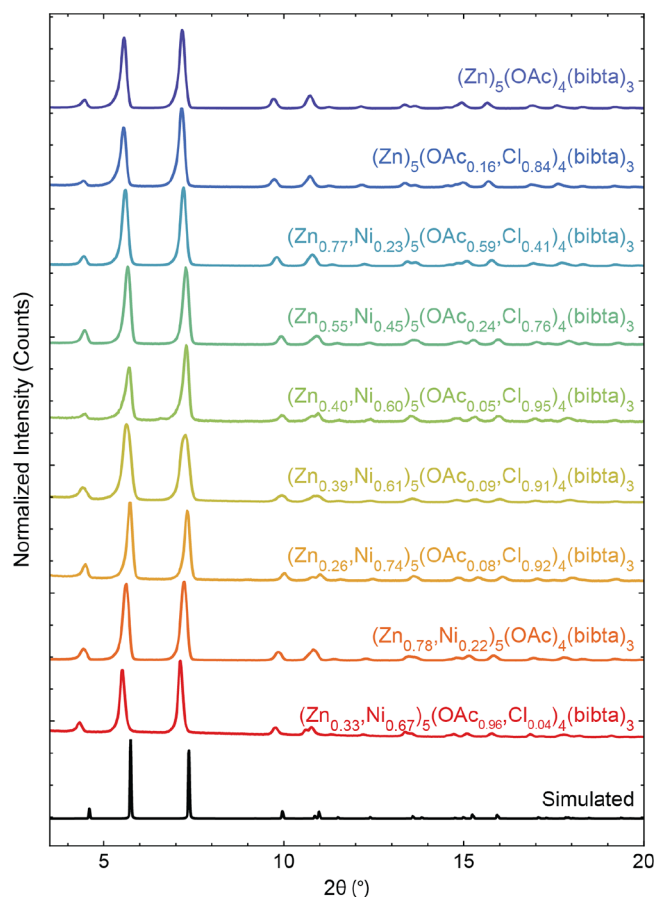


**Figure 2.** PXRD patterns of the  $(\text{Zn}_{1-x}\text{Ni}_x)_5(\text{OAc}_{1-y}\text{Cl}_{0.9y})_4(\text{bibta})_3$  series ( $0 \leq x, y \leq 1$ ).

$\text{OAc} = \text{acetate}$ ) was synthesized according to the literature procedure, by solvothermal synthesis in both  $N,N$ -dimethylformamide (DMF) and  $N$ -methylformamide (NMF).<sup>11,12</sup> These materials display similar crystallinity, porosity ( $\text{N}_2$  BET surface areas of  $2,171$  and  $2,180 \text{ m}^2/\text{g}$  and pore volumes of  $0.84$  and  $0.85 \text{ cm}^3/\text{g}$ , respectively; theoretical  $2,140 \text{ m}^2/\text{g}$  and  $0.88 \text{ cm}^3/\text{g}$ ), and water sorption behavior (relative humidity at half-capacity,  $\alpha = 50$  and  $51\%$ , respectively) (Figures S4.9, S5.1–5.2, 6.2–6.5). However, there are slight differences in the morphology of the materials, which have downstream impacts on the water sorption properties. The altitude of the triangular crystal face in the  $a$ - $b$  plane is approximately 4 times larger in the NMF crystallites ( $23.00 \pm 2.30 \mu\text{m}$ ) compared to the DMF crystallites ( $6.29 \pm 1.17 \mu\text{m}$ ) (Supplemental Section 11). We have found that the larger NMF-derived crystals are more hydrolytically stable than the DMF-derived crystals, potentially due to improved response to the stress caused by surface tension during water desorption, although the effect of synthesis conditions on water stability remains under investigation. After one water adsorption–desorption cycle, the DMF-derived material's surface area drops to  $905 \text{ m}^2/\text{g}$ , whereas that of the NMF-derived material only decreases to  $1,318 \text{ m}^2/\text{g}$  (Figure S5.1–S5.2). Due to the diminished water degradation of the NMF-derived materials,

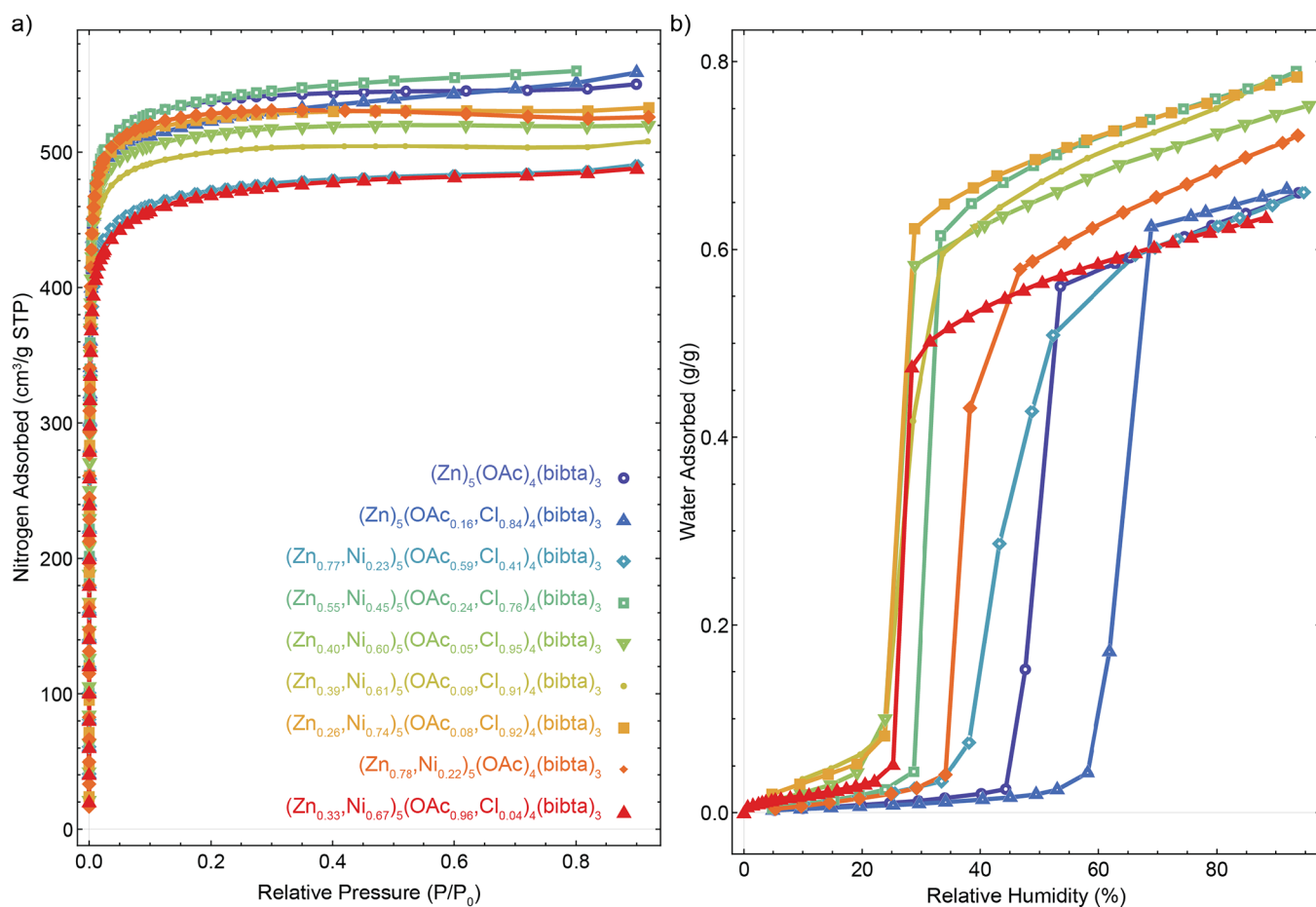


Figure 3. (a)  $N_2$  sorption isotherms measured at 77K and (b) water isotherms at 25 °C for the  $(Zn_{1-x}Ni_x)_5(OAc_{1-y}Cl_y)_4(bibta)_3$  MOF series.

Table 1. List of MOFs with Ni%, Cl%, and  $\alpha$  and Note on Stability; the Second Isotherms Are Measured after Activation at Room Temperature

shorthand name	formula unit	$\alpha$ (RH %)	surface area (first isotherm/ second isotherm) ( $m^2/g$ )	max measured water capacity (first isotherm/second isotherm) (g/g)	note
CFA-1	$(Zn)_5(OAc)_4(bibta)_3$	50	2182/1315	0.66/0.46	unstable, 30% decrease in capacity after 1 cycle
[ZnCl]	$(Zn)_5(OAc_{0.16}Cl_{0.84})_4(bibta)_3$	64	2145/1853	0.66/0.57	unstable, 14% decrease in capacity after 1 cycle
[Ni(23%),Cl(41%)]	$(Zn_{0.77}Ni_{0.23})_5(OAc_{0.59}Cl_{0.41})_4(bibta)_3$	45	1900/1829	0.66/0.64	stable, minimal loss in capacity after 2 cycles
[Ni(45%),Cl(76%)]	$(Zn_{0.55}Ni_{0.45})_5(OAc_{0.24}Cl_{0.76})_4(bibta)_3$	32	2187/2100	0.79/0.78	stable, minimal loss in capacity after 2 cycles
[Ni(60%),Cl(95%)]	$(Zn_{0.40}Ni_{0.60})_5(OAc_{0.05}Cl_{0.95})_4(bibta)_3$	27	2099/1993	0.76/0.78	stable to >80 cycles, 1.9% decrease in capacity
[Ni(61%),Cl(91%)]	$(Zn_{0.39}Ni_{0.61})_5(OAc_{0.09}Cl_{0.91})_4(bibta)_3$	29	2039/1857	0.78/0.75	stable, minimal loss in capacity after 2 cycles
[Ni(74%),Cl(92%)]	$(Zn_{0.26}Ni_{0.74})_5(OAc_{0.08}Cl_{0.92})_4(bibta)_3$	27	2147/2007	0.78/0.78	stable to >450 cycles, 5.7% decrease in capacity
[NiOAc-low]	$(Zn_{0.78}Ni_{0.22})_5(OAc)_4(bibta)_3$	38	2156/1900	0.72/0.68	stable, minimal loss in capacity after 2 cycles
[NiOAc-high]	$(Zn_{0.33}Ni_{0.67})_5(OAc_{0.96}Cl_{0.04})_4(bibta)_3$	27	1859/1741	0.63/0.60	stable, minimal loss in capacity after 2 cycles

all subsequent experiments were prepared using the NMF procedure.

Similar to the detailed postsynthetic metal exchange of Zn to Co,<sup>11</sup> proof of concept exchange of Zn to Ni,<sup>9</sup> and control over the relative humidity for pore condensation in MFU-4l by postsynthetic exchange of Zn to Co,<sup>6</sup> we recognized that detailed control of exchange of the Zn sites in CFA-1, as well

as exchange of the nonstructural anion sites, could give rise to tunable water sorption. By performing the exchange at variable temperature with varying concentrations of  $NiCl_2 \cdot 6H_2O$  in DMF, we were able to precisely control the nickel and chloride extent of exchange while maintaining crystallinity and porosity (Figures 2 and 3a). The resultant materials were isolated with a nickel loading ranging from 23 to 74% and a chloride loading

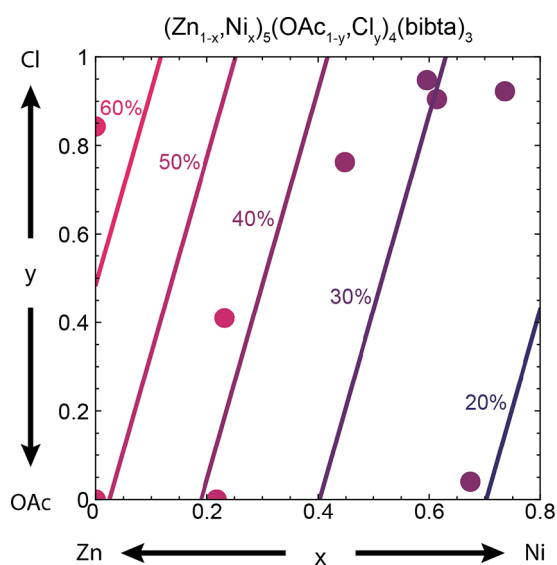


**Figure 4.** Phase space is  $\alpha$  (the relative humidity for pore condensation). The circles represent experimentally measured values, with the color indicating the value of  $\alpha$ . The solid lines are best fits to the equation,  $\ln \alpha = c_1 + \frac{5}{4}c_2x + c_3y$ , where  $c_1 = 3.95 \pm 0.07$ ,  $c_2 = -1.08 \pm 0.13$ ,  $c_3 = 0.31 \pm 0.11$ ,  $R^2 = 0.990$ .

ranging from 41 to 95%. Utilizing a technique described previously,<sup>13</sup> we have estimated the exchange thermodynamics of  $\text{NiCl}_2 \cdot 6\text{H}_2\text{O}$  at  $\Delta H^\circ = 10.1 \pm 1.8$  kcal/mol and  $\Delta S^\circ = 29.2$

$\pm 3.8$  cal/mol•K (Supplemental Discussion 8). We note that the assumption that activity coefficients are unity in the calculation of thermodynamic parameters is not strictly valid, leading to some nonlinear deviations from ideality when the concentration of nickel in solution is changed. Regardless, we find that the thermodynamic parameters offer a qualitatively useful guide for the determination of synthetic conditions to achieve a particular extent of exchange (Figure S8.2).

There may be significant diffusion limitation during postsynthetic exchanges that must be avoided. Exchange in the absence of stirring leads to materials with water isotherms containing two steps of pore condensation, consistent with the inhomogeneous distribution of nickel within the material (Figure S6.16). As such, it is critical that postsynthetic exchanges are done with stirring.

By performing multiple postsynthetic metal exchanges onto the same sample, the maximal conversion of metal exchange was determined to be 80% (Supplemental Discussion 8). This extent of exchange is consistent with complete exchange of the tetrahedral sites with no exchange of the central octahedral site. This observation is consistent with the maximum extent of postsynthetic metal exchange of cobalt into CFA-1.<sup>11</sup> As the extent of nickel exchange increases, the extent of chloride also increases (with a sigmoidal functional form; Figure S8.3). The nonlinear increase of chloride content with nickel content suggests a more complicated equilibrium in which there is a distribution of chloride and acetate over the nickel and zinc centers. This nonlinearity highlights the importance of independent synthetic control over the metal and non-

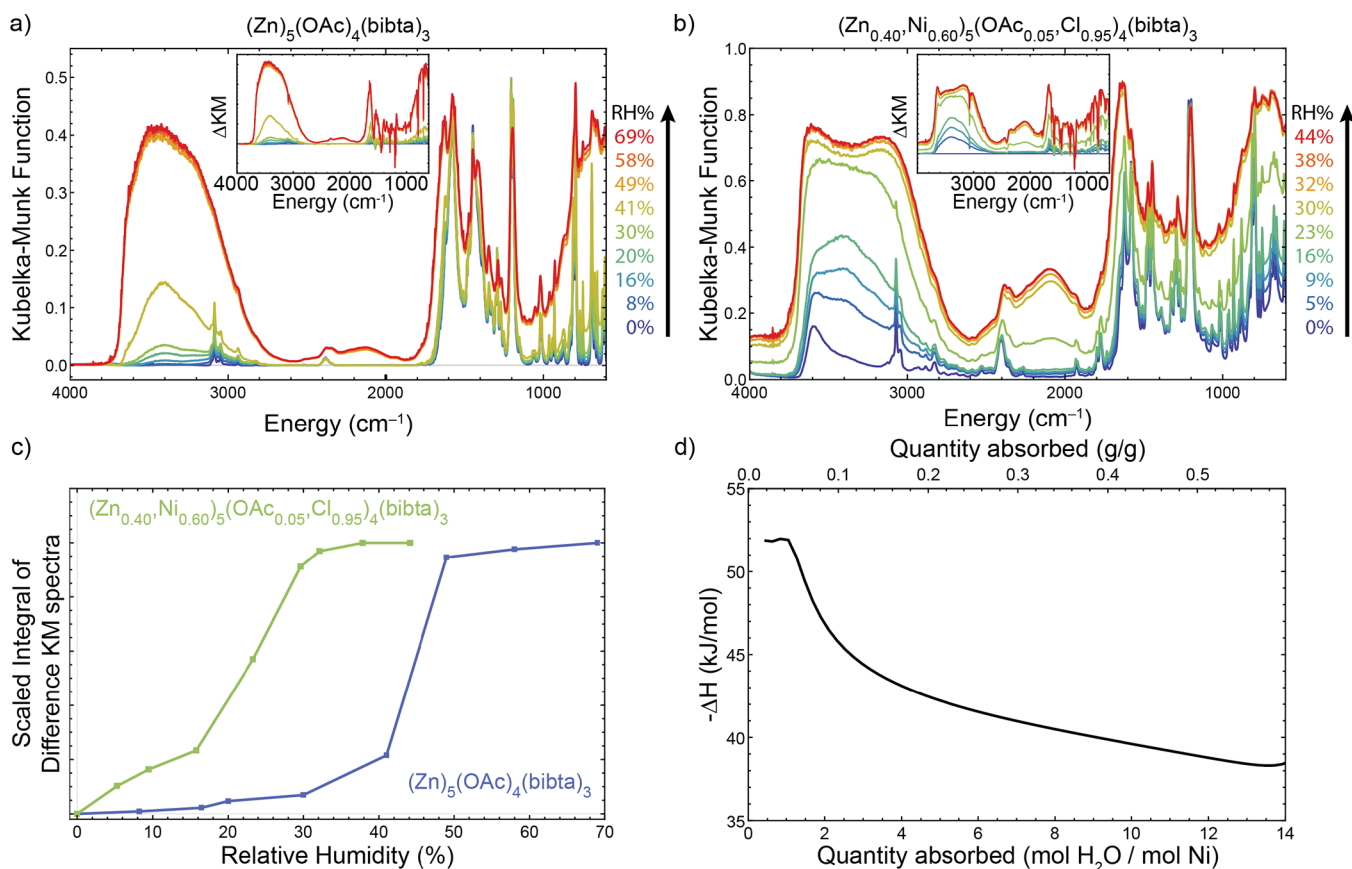


**Figure 5.** IR spectra with water dosing in (a)  $(\text{Zn})_5(\text{OAc})_4(\text{bibta})_3$  and (b)  $(\text{Zn}_{0.40}, \text{Ni}_{0.60})_5(\text{OAc}_{0.05}, \text{Cl}_{0.95})_4(\text{bibta})_3$  with (c) integrated difference spectra. (d) Isothermic enthalpy of adsorption for water in  $(\text{Zn}_{0.40}, \text{Ni}_{0.60})_5(\text{OAc}_{0.05}, \text{Cl}_{0.95})_4(\text{bibta})_3$ .

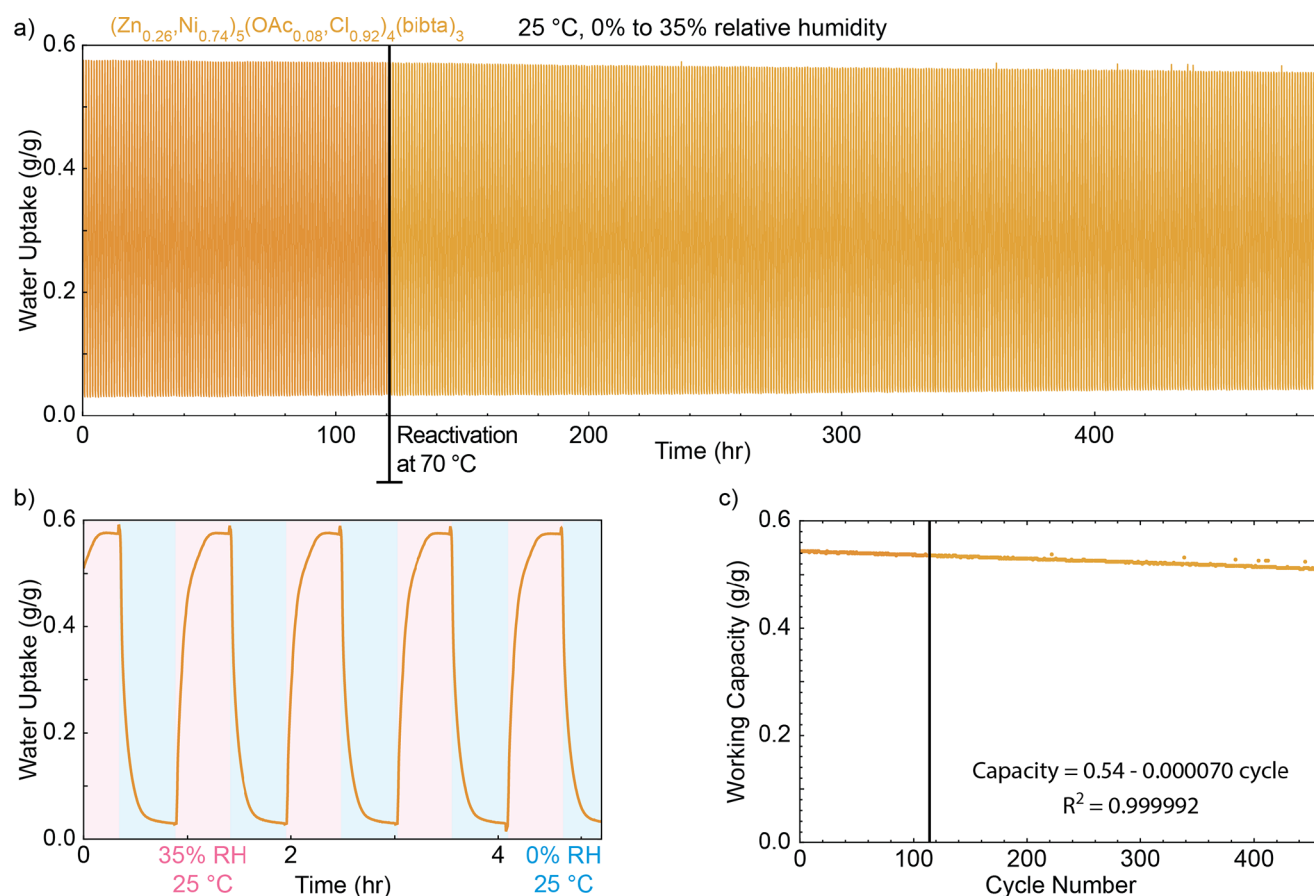


**Figure 6.** (a) Cycling  $(\text{Zn}_{0.26}\text{Ni}_{0.74})_5(\text{OAc}_{0.08}\text{Cl}_{0.92})_4(\text{bibta})_3$  framework between 0 and 35% relative humidity held at 25 °C over 450 cycles. The sample was reactivated at 70 °C after 113 cycles. (b) Magnification of the first five cycles. (c) Working capacity over the 450 cycles along with a linear fit.

structural anion content, in order to affect any resultant properties of the material. To this point, we developed new postsynthetic exchange methodologies using  $\text{ZnCl}_2$ ,  $\text{LiOAc}$ , as well as  $\text{Ni}(\text{OAc})_2$  as exchange partners, to increase chloride content or acetate content independently.

The exchange with  $\text{ZnCl}_2$  was performed at 80 °C with a large excess of  $\text{ZnCl}_2$  in order to drive the reaction forward ( $K_{\text{eq}} < 1$ ). A material with the composition  $(\text{Zn})_5(\text{OAc}_{0.16}\text{Cl}_{0.84})_4(\text{bibta})_3$  was isolated with no loss in crystallinity, a  $\text{N}_2$  BET surface area of 2,145  $\text{m}^2/\text{g}$ , and a pore volume of 0.86  $\text{cm}^3/\text{g}$ . In order to generate an acetate-rich Ni-bearing framework, we applied two different methodologies. First, the parent CFA-1 was subjected to an exchange with  $\text{Ni}(\text{OAc})_2$ , in a fashion similar to the exchange with  $\text{NiCl}_2$ . This exchange is successful at low conversions, allowing for the isolation of  $(\text{Zn}_{0.78}\text{Ni}_{0.22})_5(\text{OAc})_4(\text{bibta})_3$  (also referred here as [NiOAc-low], the full naming convention is listed in Table 1). However, when they are allowed to run at higher conversions in concentrated solutions of  $\text{Ni}(\text{OAc})_2$  in DMF, exchanges with the metal salts have a tendency to form gels. To circumvent this issue, we performed sequential exchanges with  $\text{NiCl}_2$  followed by  $\text{LiOAc}$ , such that there would never be a simultaneous high concentration of both nickel and acetate in the same reaction vessel. Utilizing this procedure, we were able to isolate  $(\text{Zn}_{0.33}\text{Ni}_{0.67})_5(\text{OAc}_{0.96}\text{Cl}_{0.04})_4(\text{bibta})_3$ . Importantly, we found no incorporation of lithium by inductively coupled plasma mass spectrometry (ICP-MS).

The metal content during postsynthetic metal exchanges was analyzed by ICP-MS. The nonstructural ion content was analyzed by digestion followed by NMR spectroscopy.<sup>9</sup> The ratio of acetate against bibta was recorded, and the fractional occupation was taken as  $1 - (\text{OAc}/12)/(\text{bibta}/18)$ . In all cases, the isolated structures maintained long-range order based on powder X-ray diffraction (PXRD) (Figure 2) and possessed porosity based on Brunauer–Emmett–Teller (BET) analysis of nitrogen adsorption isotherms at 77 K (Figure 3a).

**Water Adsorption Measurements.** Water vapor adsorption isotherms measured at 298 K for each of the  $(\text{Zn}_{1-x}\text{Ni}_x)_5(\text{OAc}_{1-y}\text{Cl}_y)_4(\text{bibta})_3$  display Heaviside step-function or sigmoidal behavior, with pore condensation occurring between 27 and 70% relative humidity (Figure 3b). For the parent  $(\text{Zn})_5(\text{OAc})_4(\text{bibta})_3$  material, the relative humidity at half-capacity,  $\alpha$ , occurs at 50% relative humidity, with a maximum capacity of 0.66 g/g. The parent material does not exhibit stable cycling behavior, with a decrease to 0.46 g/g of maximum capacity during the second cycle (Figure S6.17) and a reduction in the BET surface area from 2182 to 1315  $\text{m}^2/\text{g}$  after water vapor exposure (Figure S5.1). Upon exchange of acetate with chloride,  $(\text{Zn})_5(\text{OAc}_{0.16}\text{Cl}_{0.84})_4(\text{bibta})_3$  exhibits a shift in pore condensation to higher values, with  $\alpha$  at 64% and the same maximum capacity of 0.66 g/g. This chloride exchanged zinc framework also exhibits poor hydrolytic stability, with a decrease in maximum capacity to 0.57 g/g during the second cycle (Figure S6.18) and a diminished BET surface area of

Table 2. Water Capacity for Selected Porous Sorbents with a Critical Relative Humidity below 30%

material	$\alpha$ (RH%)	capacity at 30% RH (g/g)	maximum gravimetric capacity (g/g)	crystal density (g/cm <sup>3</sup> )	maximum volumetric capacity (cm <sup>3</sup> /cm <sup>3</sup> )	note on stability
[Ni(74%),Cl(92%)] <sup>a</sup>	27	0.63	0.78	0.73	0.57	5.7% decrease in working capacity after 450 cycles (79 cycles/1% loss)
[Ni(60%),Cl(95%)] <sup>a</sup>	27	0.60	0.75	0.73	0.55	1.9% decrease in working capacity after 80 cycles (42 cycles/1% loss)
Ni <sub>2</sub> Cl <sub>2</sub> BTDD <sup>15,26</sup>	29–32%	1.00	1.14	0.64	0.73	2% decrease in working capacity over 400 cycles (200 cycles/1% loss)
Co <sub>2</sub> Cl <sub>2</sub> BTDD <sup>2</sup>	29	0.87	0.97	0.65	0.63	6.3% decrease in working capacity over 30 cycles (4.8 cycles/1% loss)
ZrMOF-PEP-1 <sup>27</sup>	30	0.62	0.83	0.81	0.67	two step sorption with ~0.62 g/g after first step. 6% decrease in working capacity over 500 cycles (83 cycles/1% loss)
Ni <sub>2</sub> Br <sub>2</sub> BTDD <sup>15</sup>	24	0.66	0.76	0.76	0.58	<5% decrease in working capacity over 400 cycles (>80 cycles/1% loss)
MOF-LA2-1 <sup>28</sup>	26	0.61	0.68	0.85	0.58	6% decrease in working capacity over 150 cycles (25 cycles/1% loss)
Ti-MIL-125-NH <sub>2</sub> <sup>29</sup>	23	0.52	0.68	0.54	0.37	No decrease in capacity after 10 cycles
MOF-841 <sup>4</sup>	22	0.51	0.51	1.05	0.54	6% decrease in capacity after 5 cycles (0.83 cycles/1% loss)
MOF-303 <sup>30</sup>	15	0.36	0.48	1.16	0.56	~1% variation over 150 cycles (>150 cycles/1% loss)
Al fumarate <sup>31,32</sup>	27	0.33	0.48	1.06	0.51	~12% decrease in isobaric capacity after 4500 cycles (375 cycles/1% loss)
MIP-200 <sup>33</sup>	18	0.39	0.45	1.17	0.53	two step sorption. 6% decrease in working capacity after 10 cycles, followed by no further loss over 40 cycles
Ni <sub>2</sub> Cl <sub>2</sub> BBTA <sup>34</sup>	3	0.35	0.4	1.1	0.44	11% decrease in working capacity after 9 cycles (0.8 cycles/1% loss)
MOF-801-P <sup>4</sup>	9	0.31	0.36	1.59	0.56	3.5% decrease in capacity after 5 cycles (1.4 cycles/1% loss)
EMM-8 <sup>35</sup>	16	0.29	0.35	1.50	0.53	3% decrease in working capacity after 30 cycles (10 cycles/1% loss)
CAU-10-H <sup>3,36</sup>	18	0.26	0.32	1.15	0.39	no loss in capacity after 10,000 cycles
ALPO-78 <sup>37</sup>	18	0.26	0.32	1.70	0.54	no cycling data reported

<sup>a</sup>This work.

1853 m<sup>2</sup>/g (Figure S5.3). The poor stability of the zinc frameworks is attributed to the comparatively more labile Zn-triazolate bonds.<sup>14</sup>

Upon exchange to 23% nickel, [Ni(23%),Cl(41%)] displays a decrease in the relative humidity of pore condensation,  $\alpha$ , at 45% relative humidity and retention of maximum capacity at 0.66 g/g. Exchanging to 45% nickel, [Ni(45%),Cl(76%)] displayed an even lower  $\alpha$  of 32% with a maximum capacity of 0.79 g/g. Exchanging to 61% nickel, [Ni(61%),Cl(91%)] displayed a  $\alpha$  of 29% and a maximum capacity of 0.78 g/g. Exchanging to 74% nickel, [Ni(74%),Cl(92%)] displayed  $\alpha$  of 27% and maximum capacity of 0.78 g/g. Additionally, an enhancement in hydrolytic stability is observed upon metal exchange, which is confirmed by the maintenance of total water uptake during the second cycling water adsorption experiments. The porosity of the materials remains intact, as confirmed by BET surface area analysis after activating the exposed water materials at room temperature under dynamic vacuum (Table 1, Figure S5.1–S5.8).

Notably, there is minimal adsorption–desorption hysteresis for all of the water isotherms, similar to adsorption in related azolate frameworks (Figure S6.1).<sup>15</sup> Minimal hysteretic loops in chemically similar materials has been ascribed to fast pore water dynamics (i.e., facile reorientation of water within the pores), potentially driven by a large number of framework hydrogen-bond acceptors.<sup>16</sup> The lack of a large hysteresis loop (and potentially the cause of fast water dynamics in related materials) concurrent with sharp water uptake may also be due to the capillary condensation occurring in a pore with a

diameter slightly larger than the critical diameter for hysteresis at the measured temperature. The critical pore diameter for capillary condensation is well-approximated by the scaling relation,  $D_c \approx 4\sigma T_c / (T_c - T)$ , where  $\sigma$  is the sorbate diameter,  $T_c$  is the critical temperature (374 °C for water), and  $T$  is the temperature for which the isotherm is measured. Above the critical pore diameter (or equivalently below the critical temperature for capillary condensation,  $T_c^{\text{cap}}$ , for a given pore diameter), capillary condensation should be accompanied by adsorption–desorption hysteresis, and the size of the hysteresis loop should increase with increasing pore diameter.<sup>17–19</sup> For pores just above the critical pore diameter, hysteretic loops may be small, and the uptake may remain sharp. For water at 25 °C, the critical pore diameter is approximately 20 Å, slightly larger than the diameter of the largest cavity in (Zn)<sub>5</sub>(OAc)<sub>4</sub>(bibta)<sub>3</sub>.

Qualitatively, we observe that upon exchange of acetate to chloride, from (Zn)<sub>5</sub>(OAc)<sub>4</sub>(bibta)<sub>3</sub> to (Zn)<sub>5</sub>(OAc<sub>0.16</sub>Cl<sub>0.84</sub>)<sub>4</sub>(bibta)<sub>3</sub>, there is an increase in  $\alpha$ , and upon exchange of Zn to Ni, as from (Zn<sub>0.77</sub>Ni<sub>0.23</sub>)<sub>5</sub>(OAc<sub>0.59</sub>Cl<sub>0.41</sub>)<sub>4</sub>(bibta)<sub>3</sub> to (Zn<sub>0.26</sub>Ni<sub>0.74</sub>)<sub>5</sub>(OAc<sub>0.08</sub>Cl<sub>0.92</sub>)<sub>4</sub>(bibta)<sub>3</sub>, there is a decrease in  $\alpha$ . There are multiple factors that can control whether a substitution will increase or decrease  $\alpha$ , including modulation of pore size, modulation of pore hydrophobicity, or a change in the number of open metal sites that can coordinate water. The uptake behavior at low relative humidity for nickel-rich frameworks suggests that the four-coordinate nickel sites can bind 1–2 equivalents of water, while the zinc sites cannot

(evidence for coordination of equivalents of water to the nickel sites is supported by the distinctive colorimetric change of the nickel-rich frameworks from red to green upon exposure to humidity; see Figure S13.1). The additional waters bound to the nickel may seed the capillary condensation at lower relative humidity as they increase pore hydrophilicity. It is likely that the acetate causes the pores to be more hydrophilic than chloride due to additional hydrogen-bonding interactions of the acetate.

**Thermodynamic Model.** In order to quantify the effect of pore modulation on the relative humidity for capillary condensation, we developed a thermodynamic model analogous to the Ostwald–Freundlich equation (also referred to as the Kelvin equation) that describes the Gibbs free energy of binding water at the solid support-pore liquid interface (relative to the bulk liquid). Within this model, the mechanism for water adsorption may be considered capillary condensation. For the  $(\text{Zn}_{1-x}\text{Ni}_x)_5(\text{OAc}_{1-y}\text{Cl}_y)_4(\text{bibta})_3$  series, in which two sites can be continuously varied between two components, the model states,

$$\ln \alpha = c_1 + c_2 x' + c_3 y$$

(see SI Section 10 for derivation;  $x' = \frac{5}{4}x$ ), where

$$c_1 = \frac{2V}{ArkT}(\Delta G_{\text{Zn}} + \Delta G_{\text{OAc}} + \Delta G_{\text{backbone}}),$$

$$c_2 = \frac{2V}{ArkT}(\Delta G_{\text{Ni}} - \Delta G_{\text{Zn}}), \quad c_3 = \frac{2V}{ArkT}(\Delta G_{\text{Cl}} - \Delta G_{\text{OAc}}), \quad \text{and}$$

$\frac{2V}{ArkT}$  is a constant determined by the volume of a molecule of water, the projected surface area of a molecule of water on the MOF-pore water interface, the radius of the MOF pore, the Boltzmann constant, and temperature. Specifically, constants  $c_2$  and  $c_3$  encode the relative difference in Gibbs free energy of binding water to one component over the other. Approximation of the prefactor  $\frac{2V}{ArkT}$  (using the kinetic diameter of water) may be used to estimate  $\Delta G$  for binding water to one component over the other component (order of magnitude approximation,  $\Delta G \approx 10$  kJ/mol). More quantitatively, the ratio  $c_2/c_3 = (\Delta G_{\text{Ni}} - \Delta G_{\text{Zn}})/(\Delta G_{\text{Cl}} - \Delta G_{\text{OAc}})$  is a physically meaningful parameter that does not depend on the prefactor. This ratio expresses the relative importance of substitution at each site. Fitting the data, we find that  $\frac{c_2}{c_3} = -3.5$ ; thus, modulation of the cation from zinc to nickel affects the strength of binding water 3.5 times more than modulation of the anion from acetate to chloride (Figure 4).

**Mechanistic Studies.** Infrared spectroscopy was used as a means to characterize the nature of the water-framework interactions as a function of the relative humidity. Infrared spectra were recorded in diffuse reflectance geometry with an inert gas carrying a controlled relative humidity flowing over the sample. The parent  $\text{Zn}_5(\text{OAc})_4(\text{bibta})_3$  displays minimal interaction with water below the critical pressure for pore condensation (50%). The difference spectra can be fit to a broad feature that grows in a  $3,385 \text{ cm}^{-1}$  and a shoulder that maintains nearly constant intensity at  $3,112 \text{ cm}^{-1}$  (Figure 5a). The spectra for the nickel-rich  $(\text{Zn}_{0.40}\text{Ni}_{0.60})_5(\text{OAc}_{0.05}\text{Cl}_{0.95})_4(\text{bibta})_3$  displays strong interaction with water below the critical pressure for pore condensation (27%), with a sharp feature at approximately  $3,600 \text{ cm}^{-1}$  (Figure 5b). The difference spectra can be deconvoluted in three Gaussian peaks at  $3,024$ ,  $3,295$ , and  $3,521 \text{ cm}^{-1}$ . It is likely that the sharp feature around  $3,600$

$\text{cm}^{-1}$  corresponds to water that is bound directly to nickel ions, which was not removed by the initial activation at room temperature under a stream of inert gas.

By integrating the entire difference spectra, we can estimate the quantity of water in the pores at each relative humidity, similar to a water isotherm (however, the extinction coefficients for the pore water are not necessarily identical), with spectral resolution (Figure 5c). The integrated difference spectra confirm the presence of water in the Ni-rich material at relative humidity below the critical pressure for pore condensation. These observations of direct water-nickel interactions are consistent with the increase in the maximum capacity for water sorption that is observed upon exchange of zinc to nickel, as there are additional binding pockets for the water to fill. An alternative possible explanation for the difference in maximum capacity could be that the Zn-rich frameworks immediately undergo partial decomposition upon initial exposure to humidity, decreasing the maximum capacity.

By performing variable temperature water isotherms for  $[\text{Ni}(60\%),\text{Cl}(95\%)]$  at 15, 25, and 35 °C, we were able to calculate the isosteric enthalpy of adsorption,  $-\Delta H$ , of water to the frameworks (Figure 5d, SI Section 9). Up to a loading of 1 mol of water per mol of Ni,  $-\Delta H$  is approximately 52 kJ/mol. Above this loading, the isosteric enthalpy of adsorption decreases within the range of 38 to 45 kJ/mol. The increased interaction strength at the lowest loading is attributed to coordination of the waters to the nickel sites, whereas the lower interaction strength at higher loadings is attributed to water molecular binding to other waters within a hydrogen bonding network. This result is in agreement with the picture put forth by infrared spectroscopy. Outstandingly, the calculated isosteric enthalpy of adsorption is close to the enthalpy of vaporization for pure water (44 kJ/mol, 25 °C).<sup>20</sup>

**Assessing the Potential of Water Adsorption Applications.** Extended cycling experiments confirmed significant differences in durability and recyclability among the various material compositions described above. Cycling of  $(\text{Zn})_5(\text{OAc})_4(\text{bibta})_3$  at 25 °C from 0 to 63% relative humidity revealed a significant loss of 12% in the maximum amount of water uptake over just 17 cycles (Figure S6.25). In contrast, cycling of  $(\text{Zn}_{0.40}\text{Ni}_{0.60})_5(\text{OAc}_{0.05}\text{Cl}_{0.95})_4(\text{bibta})_3$  at 25 °C from 0 to 35% relative humidity reveals minimal loss (1.9%) in working capacity for over 80 cycles (Figure S6.26). The feasibility of using  $[\text{Ni}(60\%),\text{Cl}(95\%)]$  for potable water production in arid regions was assessed by subjecting the MOF to a cycle of simulated desert day and night conditions. The daytime conditions included a temperature of 45 °C and a relative humidity of 5%, while the nighttime conditions were set at 25 °C and a relative humidity of 35%. Notably, the kinetics for desorption are dramatically improved upon elevation to 45 °C (Figure S6.26c). The study showed that the MOF initially had a deliverable water capacity of 0.6 g/g. Comparatively, an extended cycling experiment for a similar high-loading Ni-based exchanged material,  $(\text{Zn}_{0.26}\text{Ni}_{0.74})_5(\text{OAc}_{0.08}\text{Cl}_{0.92})_4(\text{bibta})_3$ , at 25 °C, with relative humidity ranging from 0 to 35%, showed only a minimal loss (5.7%) in working capacity after more than 450 cycles (Figure 6). The higher stability of the nickel rich materials is attributed to the more kinetically inert Ni-triazolate bonds as compared to the Zn-triazolate bonds.<sup>14</sup> An additional remarkable feature of these materials is their ability to release adsorbed water molecules at room temperature simply by reducing the relative humidity without requiring any heating to elevated temper-

atures. This portends a cost-effective and energy-efficient recycling process.

In comparison to other strategies, the incorporation of uniformly distributed strongly adsorbing Ni sites into this material offers additional advantages by enhancing the stability and overall capacity of the material while also allowing for flexibility in adjusting the operational relative humidity range.<sup>8,21</sup> Further, we evaluated the water adsorption uptake of  $(\text{Zn}_{0.40}, \text{Ni}_{0.60})_5(\text{OAc}_{0.05}, \text{Cl}_{0.95})_4(\text{bibta})_3$  and  $(\text{Zn}_{0.26}, \text{Ni}_{0.74})_5(\text{OAc}_{0.08}, \text{Cl}_{0.92})_4(\text{bibta})_3$  in comparison with the best performing materials for water capture with  $\alpha$  below 30% RH (Table 2). The results demonstrated that these materials ranked among the top adsorbents in terms of their high adsorption capacity at low humidity levels (Figure S7.1). Critically, this low humidity regime between 10 and 30% relative humidity is useful for atmospheric water harvesting.<sup>22</sup> Sorbents have a higher efficiency than dew plates, fog nets, and membranes systems for water harvesting in the regime of  $\sim 20$ – $30$  °C at 20–30% relative humidity, as well as higher efficiency than both dew plates and fog nets in the 10–20% relative humidity at the same temperature range.<sup>23</sup>

The capability of modulating the relative humidity for pore condensation of  $\text{M}_3\text{X}_4(\text{bibta})_3$  also offers the possibility for designing a multistage dehumidification system.<sup>24,25</sup> Given the relatively fast kinetics for sorption, minimal hysteresis, and high capacity, it should be possible to design a multistage desiccant wheel system in which each stage in the system uptakes water at a progressively lower relative humidity. However, the cycling stability of the materials in the higher relative humidity regime must be improved.

## CONCLUSIONS

In summary, the systematic synthetic modifications of the  $(\text{Zn}_{1-x}, \text{Ni}_x)_5(\text{OAc}_{1-y}, \text{Cl}_y)_4(\text{bibta})_3$  MOF platform advance our fundamental knowledge of water adsorption in confined space. Moreover, they introduce a promising class of new adsorbent compositions characterized by their high water capacity, particularly at low relative humidity levels (<30%). These synthetically scalable adsorbents further exhibit remarkable long-term stability, emphasizing their potential for practical applications.

The approach presented in this study offers the opportunity to extend its findings to incorporate various hydrophobic and hydrophilic anions. The introduction of nickel as a modulating cation enables the adjustment of the relative humidity range in which water uptake occurs and enhances the hydrolytic stability of the new MOFs. As described there, the particular platform involving bibta ligands holds potential for a wide range of water sorption applications. By expanding our understanding of water confinement and leveraging the ability to tailor material properties, this research opens new avenues for the development of advanced materials with enhanced water sorption capacities.

## ASSOCIATED CONTENT

### Supporting Information

The Supporting Information is available free of charge at <https://pubs.acs.org/doi/10.1021/jacs.3c08335>.

Elemental analysis, PXRD,  $\text{N}_2$  isotherms,  $\text{H}_2\text{O}$  isotherms, isosteric enthalpy of adsorption calculation, thermodynamic calculations, synthetic procedures, SEM, and photographs (PDF)

AIF files (ZIP)

## AUTHOR INFORMATION

### Corresponding Author

Mircea Dincă – Department of Chemistry, Massachusetts Institute of Technology, Cambridge, Massachusetts 02139, United States; [orcid.org/0000-0002-1262-1264](https://orcid.org/0000-0002-1262-1264); Email: [mdinca@mit.edu](mailto:mdinca@mit.edu)

### Authors

Dalal Alezi – Department of Chemistry, Faculty of Science, King Abdulaziz University, Jeddah 21441, Saudi Arabia; Department of Chemistry, Massachusetts Institute of Technology, Cambridge, Massachusetts 02139, United States; [orcid.org/0000-0002-3462-1193](https://orcid.org/0000-0002-3462-1193)

Julius J. Oppenheim – Department of Chemistry, Massachusetts Institute of Technology, Cambridge, Massachusetts 02139, United States; [orcid.org/0000-0002-5988-0677](https://orcid.org/0000-0002-5988-0677)

Patrick J. Sarver – Department of Chemistry, Massachusetts Institute of Technology, Cambridge, Massachusetts 02139, United States; [orcid.org/0000-0001-7227-8966](https://orcid.org/0000-0001-7227-8966)

Andrei Iliescu – Department of Chemistry, Massachusetts Institute of Technology, Cambridge, Massachusetts 02139, United States; [orcid.org/0000-0002-2076-1566](https://orcid.org/0000-0002-2076-1566)

Bhavish Dinakar – Department of Chemical Engineering, Massachusetts Institute of Technology, Cambridge, Massachusetts 02139, United States; [orcid.org/0000-0002-7611-101X](https://orcid.org/0000-0002-7611-101X)

Complete contact information is available at: <https://pubs.acs.org/doi/10.1021/jacs.3c08335>

### Author Contributions

<sup>†</sup>D.A., J.J.O., and P.J.S. contributed equally. The manuscript was written through contributions of all authors. All authors have given approval to the final version of the manuscript.

### Funding

This research was funded by the Brown Science Foundation. P.J.S. thanks the National Institute of General Medical Sciences of the National Institutes of Health for postdoctoral fellowship support (F32 GM147937). The content is solely the responsibility of the authors and does not necessarily represent the official views of the National Institutes of Health. D.A. thanks the KACST-MIT Ibn Khaldun Fellowship for fellowship support.

### Notes

The authors declare no competing financial interest.

## ACKNOWLEDGMENTS

We would like to thank Dr. Gang Liu for assistance repairing instrumentation and Professor Francesco Paesani for helpful discussion.

## REFERENCES

- (1) Towsif Abtab, S. M.; Alezi, D.; Bhatt, P. M.; Shkurenko, A.; Belmabkhout, Y.; Aggarwal, H.; Weseliński, E. J.; Alsadun, N.; Samin, U.; Hedhili, M. N.; Eddaoudi, M. Reticular Chemistry in Action: A Hydrolytically Stable MOF Capturing Twice Its Weight in Adsorbed Water. *Chem.* **2018**, *4* (1), 94–105.
- (2) Rieth, A. J.; Yang, S.; Wang, E. N.; Dincă, M. Record Atmospheric Fresh Water Capture and Heat Transfer with a Material Operating at the Water Uptake Reversibility Limit. *ACS Cent. Sci.* **2017**, *3* (6), 668–672.

- (3) Fröhlich, D.; Pantatosaki, E.; Kolokathis, P. D.; Markey, K.; Reinsch, H.; Baumgartner, M.; van der Veen, M. A.; De Vos, D. E.; Stock, N.; Papadopoulos, G. K.; Henninger, S. K.; Janiak, C. Water Adsorption Behaviour of CAU-10-H: A Thorough Investigation of Its Structure–Property Relationships. *J. Mater. Chem. A* **2016**, *4* (30), 11859–11869.
- (4) Furukawa, H.; Gándara, F.; Zhang, Y.-B.; Jiang, J.; Queen, W. L.; Hudson, M. R.; Yaghi, O. M. Water Adsorption in Porous Metal–Organic Frameworks and Related Materials. *J. Am. Chem. Soc.* **2014**, *136* (11), 4369–4381.
- (5) Ko, N.; Choi, P. G.; Hong, J.; Yeo, M.; Sung, S.; Cordova, K. E.; Park, H. J.; Yang, J. K.; Kim, J. Tailoring the Water Adsorption Properties of MIL-101 Metal–Organic Frameworks by Partial Functionalization. *J. Mater. Chem. A* **2015**, *3* (5), 2057–2064.
- (6) Wright, A. M.; Rieth, A. J.; Yang, S.; Wang, E. N.; Dincă, M. Precise Control of Pore Hydrophilicity Enabled by Post-Synthetic Cation Exchange in Metal–Organic Frameworks. *Chem. Sci.* **2018**, *9* (15), 3856–3859.
- (7) Hanikel, N.; Pei, X.; Chheda, S.; Lyu, H.; Jeong, W.; Sauer, J.; Gagliardi, L.; Yaghi, O. M. Evolution of Water Structures in Metal–Organic Frameworks for Improved Atmospheric Water Harvesting. *Science* **2021**, *374* (6566), 454–459.
- (8) Zheng, Z.; Hanikel, N.; Lyu, H.; Yaghi, O. M. Broadly Tunable Atmospheric Water Harvesting in Multivariate Metal–Organic Frameworks. *J. Am. Chem. Soc.* **2022**, *144* (49), 22669–22675.
- (9) Bien, C. E.; Liu, Q.; Wade, C. R. Assessing the Role of Metal Identity on CO<sub>2</sub> Adsorption in MOFs Containing M–OH Functional Groups. *Chem. Mater.* **2020**, *32* (1), 489–497.
- (10) Coffin, D. R.; Serad, G. A.; Hicks, H. L.; Montgomery, R. T. Properties and Applications of Celanese PBI–Polybenzimidazole Fiber. *Text. Res. J.* **1982**, *52* (7), 466–472.
- (11) Schmieder, P.; Denysenko, D.; Grzywa, M.; Baumgärtner, B.; Senkovska, I.; Kaskel, S.; Sastre, G.; van Willen, L.; Volkmer, D. CFA-1: The First Chiral Metal–Organic Framework Containing Kuratowski-Type Secondary Building Units. *Dalton Trans.* **2013**, *42* (30), 10786–10797.
- (12) Bien, C. E.; Chen, K. K.; Chien, S.-C.; Reiner, B. R.; Lin, L.-C.; Wade, C. R.; Ho, W. S. W. Bioinspired Metal–Organic Framework for Trace CO<sub>2</sub> Capture. *J. Am. Chem. Soc.* **2018**, *140* (40), 12662–12666.
- (13) Brozek, C. K.; Dincă, M. Thermodynamic Parameters of Cation Exchange in MOF-5 and MFU-4l. *Chem. Commun.* **2015**, *51* (59), 11780–11782.
- (14) Rieth, A. J.; Wright, A. M.; Dincă, M. Kinetic Stability of Metal–Organic Frameworks for Corrosive and Coordinating Gas Capture. *Nat. Rev. Mater.* **2019**, *4* (11), 708–725.
- (15) Rieth, A. J.; Wright, A. M.; Skorupskii, G.; Mancuso, J. L.; Hendon, C. H.; Dincă, M. Record-Setting Sorbents for Reversible Water Uptake by Systematic Anion Exchanges in Metal–Organic Frameworks. *J. Am. Chem. Soc.* **2019**, *141* (35), 13858–13866.
- (16) Valentine, M. L.; Yin, G.; Oppenheim, J. J.; Dincă, M.; Xiong, W. Ultrafast Water H-Bond Rearrangement in a Metal–Organic Framework Probed by Femtosecond Time-Resolved Infrared Spectroscopy. *J. Am. Chem. Soc.* **2023**, *145* (21), 11482–11487.
- (17) Coasne, B.; Gubbins, K. E.; Pellenq, R. J.-M. Temperature Effect on Adsorption/Desorption Isotherms for a Simple Fluid Confined within Various Nanopores. *Adsorption* **2005**, *11* (1), 289–294.
- (18) Morishige, K.; Fujii, H.; Uga, M.; Kinukawa, D. Capillary Critical Point of Argon, Nitrogen, Oxygen, Ethylene, and Carbon Dioxide in MCM-41. *Langmuir* **1997**, *13* (13), 3494–3498.
- (19) Ball, P. C.; Evans, R. Temperature Dependence of Gas Adsorption on a Mesoporous Solid: Capillary Criticality and Hysteresis. *Langmuir* **1989**, *5* (3), 714–723.
- (20) The Engineering ToolBox 2010. *Water - Heat of Vaporization vs. Temperature*. [https://www.engineeringtoolbox.com/water-properties-d\\_1573.html](https://www.engineeringtoolbox.com/water-properties-d_1573.html).
- (21) Schlüsener, C.; Xhinovci, M.; Ernst, S.-J.; Schmitz, A.; Tannert, N.; Janiak, C. Solid-Solution Mixed-Linker Synthesis of Isorecticular Al-Based MOFs for an Easy Hydrophilicity Tuning in Water-Sorption Heat Transformations. *Chem. Mater.* **2019**, *31* (11), 4051–4062.
- (22) Liu, X.; Wang, X.; Kapteijn, F. Water and Metal–Organic Frameworks: From Interaction toward Utilization. *Chem. Rev.* **2020**, *120* (16), 8303–8377.
- (23) Rao, A. K.; Fix, A. J.; Yang, Y. C.; Warsinger, D. M. Thermodynamic Limits of Atmospheric Water Harvesting. *Energy Environ. Sci.* **2022**, *15* (10), 4025–4037.
- (24) Shahvari, S. Z.; Clark, J. D. Approaching Theoretical Maximum Energy Performance for Desiccant Dehumidification Using Staged and Optimized Metal–Organic Frameworks. *Appl. Energy* **2023**, *331*, No. 120421.
- (25) Zhang, B.; Zhu, Z.; Wang, X.; Liu, X.; Kapteijn, F. Water Adsorption in MOFs: Structures and Applications. *Adv. Funct. Mater.* **2023**, 2304788.
- (26) Bagi, S.; Wright, A. M.; Oppenheim, J.; Dincă, M.; Román-Leshkov, Y. Accelerated Synthesis of a Ni<sub>2</sub>Cl<sub>2</sub>(BTDD) Metal–Organic Framework in a Continuous Flow Reactor for Atmospheric Water Capture. *ACS Sustain. Chem. Eng.* **2021**, *9* (11), 3996–4003.
- (27) Liu, W.; Wu, E.; Yu, B.; Liu, Z.; Wang, K.; Qi, D.; Li, B.; Jiang, J. Reticular Synthesis of Metal–Organic Frameworks by 8-Connected Quadrangular Prism Ligands for Water Harvesting. *Angew. Chem., Int. Ed.* **2023**, *62* (33), No. e202305144.
- (28) Hanikel, N.; Kurandina, D.; Chheda, S.; Zheng, Z.; Rong, Z.; Neumann, S. E.; Sauer, J.; Siepmann, J. I.; Gagliardi, L.; Yaghi, O. M. MOF Linker Extension Strategy for Enhanced Atmospheric Water Harvesting. *ACS Cent. Sci.* **2023**, *9* (3), 551–557.
- (29) Sohail, M.; Yun, Y.-N.; Lee, E.; Kim, S. K.; Cho, K.; Kim, J.-N.; Kim, T. W.; Moon, J.-H.; Kim, H. Synthesis of Highly Crystalline NH<sub>2</sub>-MIL-125 (Ti) with S-Shaped Water Isotherms for Adsorption Heat Transformation. *Cryst. Growth Des.* **2017**, *17* (3), 1208–1213.
- (30) Fathieh, F.; Kalmutzki, M. J.; Kapustin, E. A.; Waller, P. J.; Yang, J.; Yaghi, O. M. Practical Water Production from Desert Air. *Sci. Adv.* **2018**, *4* (6), No. eaat3198.
- (31) de Lange, M. F.; Verouden, K. J. F. M.; Vlucht, T. J. H.; Gascon, J.; Kapteijn, F. Adsorption-Driven Heat Pumps: The Potential of Metal–Organic Frameworks. *Chem. Rev.* **2015**, *115* (22), 12205–12250.
- (32) Jeremias, F.; Fröhlich, D.; Janiak, C.; Henninger, K. S. Advancement of Sorption-Based Heat Transformation by a Metal Coating of Highly-Stable, Hydrophilic Aluminium Fumarate MOF. *RSC Adv.* **2014**, *4* (46), 24073–24082.
- (33) Wang, S.; Lee, J. S.; Wahiduzzaman, M.; Park, J.; Muschi, M.; Martineau-Corcoss, C.; Tissot, A.; Cho, K. H.; Marrot, J.; Shepard, W.; Maurin, G.; Chang, J.-S.; Serre, C. A Robust Large-Pore Zirconium Carboxylate Metal–Organic Framework for Energy-Efficient Water-Sorption-Driven Refrigeration. *Nat. Energy* **2018**, *3* (11), 985–993.
- (34) Rieth, A. J.; Wright, A. M.; Rao, S.; Kim, H.; LaPotin, A. D.; Wang, E. N.; Dincă, M. Tunable Metal–Organic Frameworks Enable High-Efficiency Cascaded Adsorption Heat Pumps. *J. Am. Chem. Soc.* **2018**, *140* (50), 17591–17596.
- (35) Liu, Z.; Xu, J.; Xu, M.; Huang, C.; Wang, R.; Li, T.; Huai, X. Ultralow-Temperature-Driven Water-Based Sorption Refrigeration Enabled by Low-Cost Zeolite-like Porous Aluminophosphate. *Nat. Commun.* **2022**, *13* (1), 193.
- (36) Solovyeva, M. V.; Shkatulov, A. I.; Gordeeva, L. G.; Fedorova, E. A.; Krieger, T. A.; Aristov, Y. I. Water Vapor Adsorption on CAU-10-X: Effect of Functional Groups on Adsorption Equilibrium and Mechanisms. *Langmuir* **2021**, *37* (2), 693–702.
- (37) Yuhás, B. D.; Mowat, J. P. S.; Miller, M. A.; Sinkler, W. ALPO-78: A 24-Layer ABC-6 Aluminophosphate Synthesized Using a Simple Structure-Directing Agent. *Chem. Mater.* **2018**, *30* (3), 582–586.